SCIENTIFIC REPORTS

OPEN

SUBJECT AREAS:
ENGINEERING
NANOSCIENCE AND TECHNOLOGY

Received
15 April 2014

Accepted
14 July 2014

Published
5 August 2014

Correspondence and requests for materials should be addressed to Y.A.H. (yahuang@hust.edu.cn) or Z.P.Y. (yinzhp@mail.hust.edu.cn)

Versatile, kinetically controlled, high precision electrohydrodynamic writing of micro/nanofibers

YongAn Huang[1], Yongqing Duan[1], Yajiang Ding[1], Ningbin Bu[1], Yanqiao Pan[1], Nanshu Lu[2] & Zhouping Yin[1]

[1]State Key Laboratory of Digital Manufacturing Equipment and Technology, Huazhong University of Science and Technology, Wuhan, 430074, China, [2]Center for Mechanics of Solids, Structures and Materials, Department of Aerospace Engineering and Engineering Mechanics, University of Texas at Austin, Austin, Texas 78712, USA.

Direct writing of hierarchical micro/nanofibers have recently gained popularity in flexible/stretchable electronics due to its low cost, simple process and high throughput. A kinetically controlled mechanoelectrospinning (MES) is developed to directly write diversified hierarchical micro/nanofibers in a continuous and programmable manner. Unlike conventional near-field electrospinning, our MES method introduces a mechanical drawing force, to simultaneously enhance the positioning accuracy and morphology controllability. The MES is predominantly controlled by the substrate speed, the nozzle-to-substrate distance, and the applied voltage. As a demonstration, smooth straight, serpentine, self-similar, and bead-on-string structures are direct-written on silicon/elastomer substrates with a resolution of 200 nm. It is believed that MES can promote the low-cost, high precision fabrication of flexible/stretchable electronics or enable the direct writing of the sacrificial structures for nanoscale lithography.

Micro/nanofibers composed of electrically conductive, semiconducting, photoelectric, piezoelectric or dielectric materials have been extensively explored as light-emitters, energy harvesters, supercapacitors and sensors[1–3]. If the electrically functional or active micro/nanofibers can be directly written on flexible substrates at low temperature, low cost flexible/stretchable electronics are expected to be fabricated without conventional photolithography processes. The direct-writing of smooth microstructures with viscous ink has attracted considerable attention in flexible/stretchable electronics[4]. Near-field electrospinning (NFES) can write smooth micro/nanofibers in a direct, continuous manner[5], to fabricate nanowire electronics, piezoelectric devices and so on, using functional or sacrificial inks[6–9]. It overcomes the drawbacks of established ink-jet technique (applying heat or piezoelectric actuator to "push" a droplet of ink[10–12]) which include limited printing resolution (20 μm[13]), incompatibility with high-viscosity electronic ink[14,15], and rugged structures due to discrete droplets. However, it is humdrum to just write straight micro/nanofibers. To write in a variety of patterns, the control of the position, resolution, and morphology of electrospun micro/nanofibers should be improved.

Here, we present a mechanoelectrospinning (MES) process that is kinetically controlled and high resolution. It utilizes the combination of electrical and mechanical forces, rather than purely electric field in NFES or thermal/acoustic energy in traditional ink-jet printing, to drive the viscous ink for the direct-writing of high-resolution, customizable microstructures. In addition to the features of ink-jet techniques such as large-area printing, low-cost operation, and customized flexibility[16–18], the MES has some unique advantages such as: 1) resolution tunable from micrometre to nanometre using nozzles of diameters larger than 100 μm, which are not easy to be jammed, 2) compatibility with inks of broad ranges of viscosity that cannot be used in established ink-jet printing or photolithography techniques, 3) simultaneous control on the position and morphology of the deposited structures, and 4) direct deposition of smooth hierarchical structures such as island-bridge structures, serpentine structures, self-similar structures, and multi-level dot-array. The writing resolution, position, morphology, and patterns can be readily tuned by digitally controlled motion stage (substrate holder), nozzle-to-substrate distance, and applied voltage. It is hence a highly versatile and low cost method to direct-write solution-based materials for large-scale flexible/stretchable electronics and soft nanolithography.

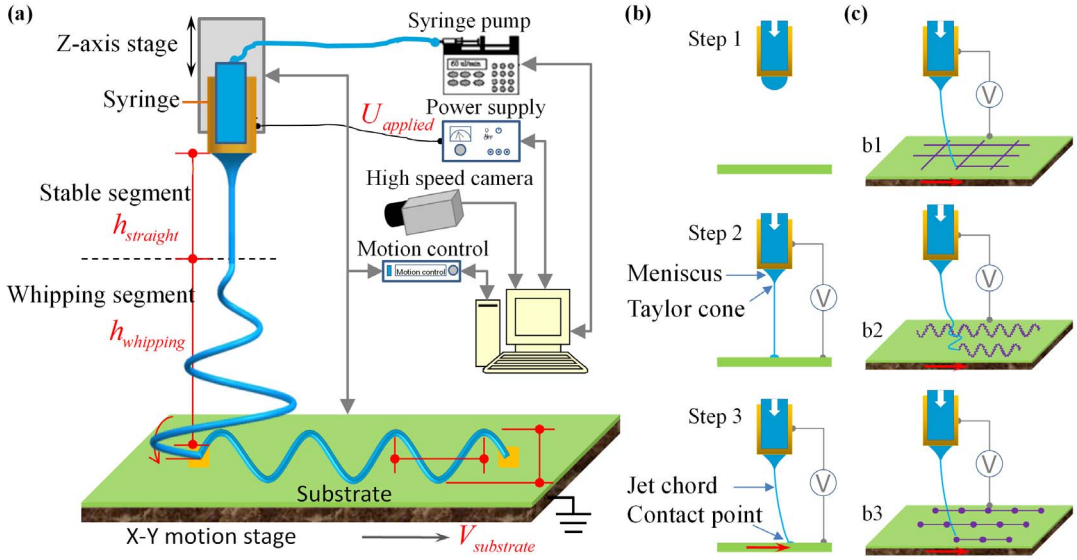

Figure 1 | Schematic of multifunctional MES direct-writing process. (a) Experimental setup and mechanism of MES direct-writing process. (b) Broken-down steps of MES direct-writing: ink is first filled in the nozzle and a drop forms at the end of the nozzle; when voltage is applied, the end drop is jetted from the nozzle and a Taylor cone is formed; when substrate starts to move, a fine 'jet chord' is formed between the meniscus and the contact point on the substrate. (c) Three modes of MES direct-writing process: the mapped direct-writing of straight structures, helix direct-writing of serpentine structures, and leap direct-writing of bead-on-string structure.

Principles and Implementation

Figure 1a shows the schematic of MES direct-writing system that merges several disparate concepts. First, MES process is able to precisely manipulate the position, size, and morphology of each electrospun micro/nanofiber by adjusting the combination of mechanical drawing force and electrical field. The mechanical drawing force is determined by the velocity of substrate holder. When the optimal combination is achieved, sub-micrometer structures can be well written. Second, the nozzle-to-substrate distance, $h_{z\text{-axis}} = h_{straight} + h_{whipping}$, is tunable from 0.5 mm to 10 mm, to fully explore the different dynamics of jetting fibers. Third, the applied voltage $U_{voltage}$ first gradually increases to a critical value to jet the ink from the apex of the Taylor cone, then decreases to a lower voltage just to stabilize the Taylor cone. Fourth, the motion stage where the substrate rests on is digitally controlled and hence stretches the jetting fiber in programmable manner. The four features make MES a versatile direct-writing technique, to fabricate abundant microstructures such as fiber array, serpentine structures and bead-on-string structures.

Figure 1b illustrates the MES process: filling nozzle with functional ink → increasing applied voltage to a high value, such as 2 kV → stretching the jetting fiber → decreasing applied voltage to a lower voltage such as 0.8 ~ 1 kV. The jetting fiber is analogous to the soft ladders dropping from helicopter, in the sense that it is impossible to control the landing point. The NFES tries to enhance positioning accuracy by shortening the nozzle-to-substrate distance. Here, an idea to achieve more precise positioning is borrowed from the kite that flies when dragged by a running person through a string. The ground position is controlled by the person, regardless of the position of the kite or the rigidity of the kite. A digitally controlled motion stage is adopted as the "person" to draw the jet micro/nanofiber. Three key processing parameters can tune the dynamic behavior of the jet fiber: 1) the translational speed, $v_{substrate}$, which controls the mechanical drawing force and hence the fiber diameter or ribbon width, 2) the nozzle-to-substrate distance, $h_{z\text{-axis}}$, which controls the cross-sectional geometry (i.e. circular or rectangular) as well as the shape (i.e. linear or serpentine) of the written structure, and 3) the applied voltage, $U_{voltage}$, which dictates the dynamic behavior of jetting, as well as the fiber diameter. The tunable mechanical drawing force plays a critical role in improving the control over fiber position and morphology. It is helpful for controlling the bending instability of jet fibers[6], and can reliably generate finer and longer fibers[19]. It is the primary cause that the electrical field of MES (about 2×10^5 V/m) is far lower than that of NFES (about 1×10^7 V/m)[5]. As a result, it helps avoid the electrical breakdown of the polymer substrates of flexible electronics during direct-writing.

The drawing force acting on the jetting fiber can be determined by the slope of the fiber θ, which increases with the translational speed (captured by a high-speed camera, see supplementary Figure S1). h_{z-axis} ranges from 0.5 ~ 10 mm, far smaller than 15 ~ 30 cm in traditional electrospinning[20,21], but larger than ~0.5 mm used inNFES[5]. In traditional electrospinning, the jet fiber completely solidifies when reaching the substrate whereas NFES adopts a solid tip, rather than a needle, to dip in a concentrated solution and then deposit a solid fiber. Adopting $0.5\ mm < h_{z-axis} < 10\ mm$ gives the following advantages: 1) solution with a wide range of concentration may be supplied continuously by a needle for large-area nonstop printing; 2) the deposited micro/nanofiber can be tuned from solid to liquid, to control the cross-sectional geometry; and 3) the jetting velocity can be easily tuned to be comparable to the motion stage, yielding reasonable mechanical drawing force.

Several variants of MES are developed by coordinating the above process parameters. 1) The mapped direct-writing (MDW) mode is developed by introducing the "near-field" method to shorten the h_{z-axis} within the range of the length of stable segment $h_{straight}$ (e.g. $h_{straight} = 5\ mm$), as shown in Figure 1a. The deposited micro/nanofibers are the mapping results of relative motion of the nozzle and substrate. 2) The leap direct-writing (LDW) mode is based on the competition between the mechanical drawing force, the electric force and the viscoelastic force, and works when $0.5\ mm < h_{z-axis} < 2\ mm$ and $v_{substrate} < 150\ mm/s$ in experiments. It is utilized to fabricate bead-on-string structures in a programmable manner. 3) The helix direct-writing (HDW) mode is resulted from the whipping/buckling effect of electrospinning, where $h_{straight} < h_{z-axis} < h_{straight} + h_{whipping}$ (e.g. $15\ mm < h_{z-axis} < 45\ mm$), where $h_{whipping}$ is the height of the first phase of instability. Serpentine structures can thereby be direct-written via linear translations of the motion stage. Complex microstructures can be generated out of the different writing modes,

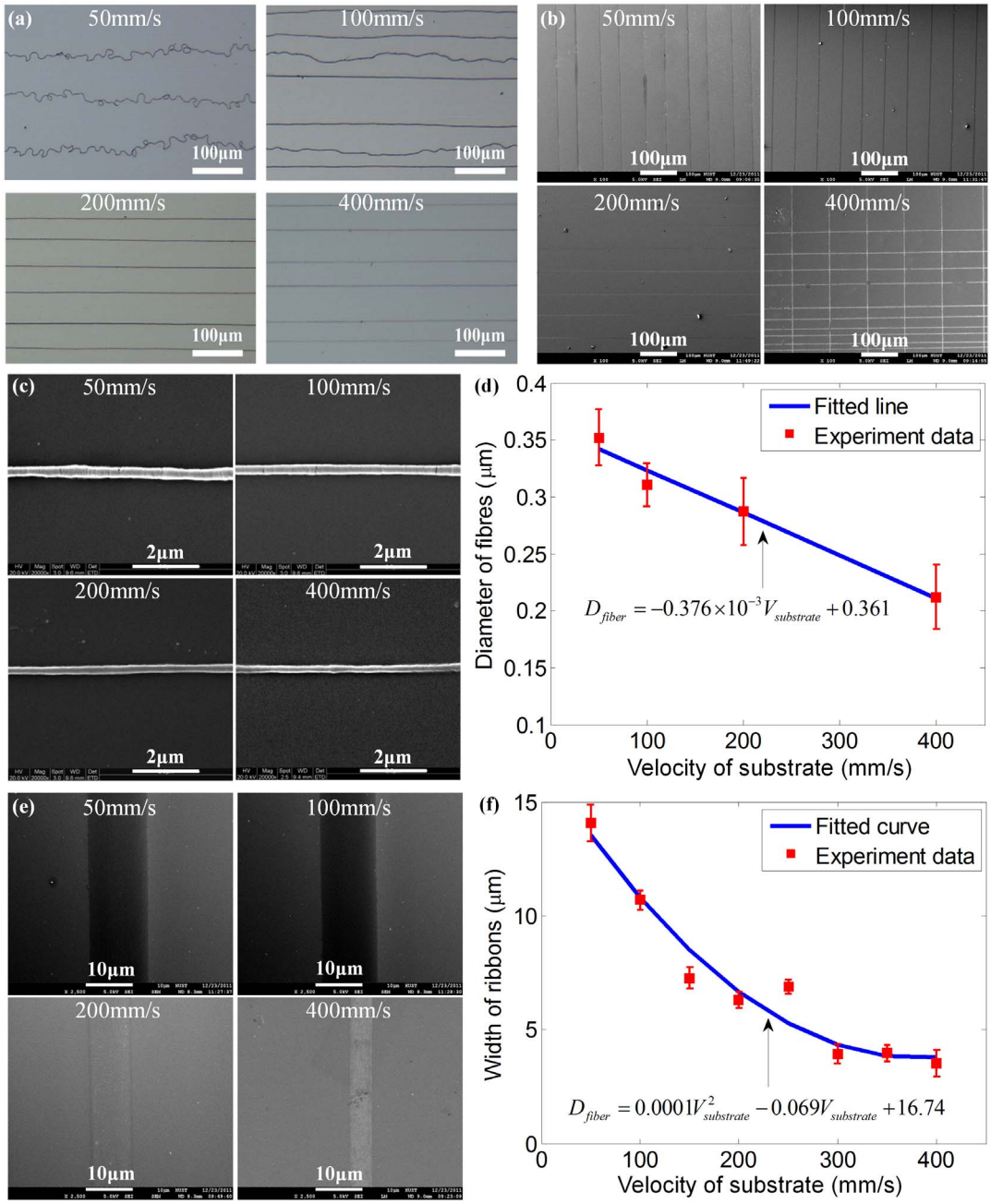

Figure 2 | The dependence of fiber-diameter or ribbon-width on the velocity of the substrate: (a) optical micrographs of direct-written fibers at speeds of 50 mm/s, 100 mm/s, 200 mm/s and 400 mm/s with 5 mm nozzle-to-substrate distance; (b) SEM images of direct-written fibers at speeds of 50 mm/s, 100 mm/s, 200 mm/s and 400 mm/s with 2 mm nozzle-to-substrate distance; (c) SEM images of aligned fiber with 5 mm nozzle-to-substrate distance at speeds of 50 mm/s, 100 mm/s, 200 mm/s and 400 mm/s; (d) Correlation between fiber-diameter and the velocity of substrate; (e) are similar with (c), but with 2 mm nozzle-to-substrate distance, and the direct-written structures are ribbons; (f) Correlation between ribbon-width and the velocity of substrate.

including large-scale straight fiber array, multi-level wavy structures, in-plane/out-of-plane buckled structures, and bead-on-string structures, as illustrated in Figure 1c. All the experiments were performed under the room temperature and relative humidity of about 25%.

Results and Discussion

Mapped direct-writing of straight micro/nanofiber and their self-assembly to form dot arrays. Mapped direct-writing mode can deposit microstructures with controllable morphology and precise position. $h_{z\text{-axis}}$ controls the dynamic behavior as well as the phase change of fibers. If $v_{substrate} > 150\ mm/s$, straight liquid ribbons and solid micro/nanofibers can be direct-written when $0.5\ mm < h_{z\text{-}axis} < 2\ mm$ and $2\ mm < h_{z\text{-}axis} < 5\ mm$, respectively. The degree of solidification can be tuned continuously, so that the cross-sectional geometry can gradually change from thin film to circle. In experiment, the ink is polyethylene oxide (PEO, M_w = 300 000) solution dissolved in distilled water with the weight concentration of 6 wt%. When $h_{z\text{-}axis} < 2\ mm$, there is not enough time for the solvent to completely evaporate before the ink reaches the substrate, hence liquid ink will rest and spread on the substrate to form a ribbon.

It is found that $v_{substrate}$ has significant influence on the positioning of electrospun micro/nanofibers. When $v_{substrate}$ is much lower than the speed of jetting, $v_{jetting}$, (e.g. $v_{jetting} \approx 170\ mm/s$ when the flow

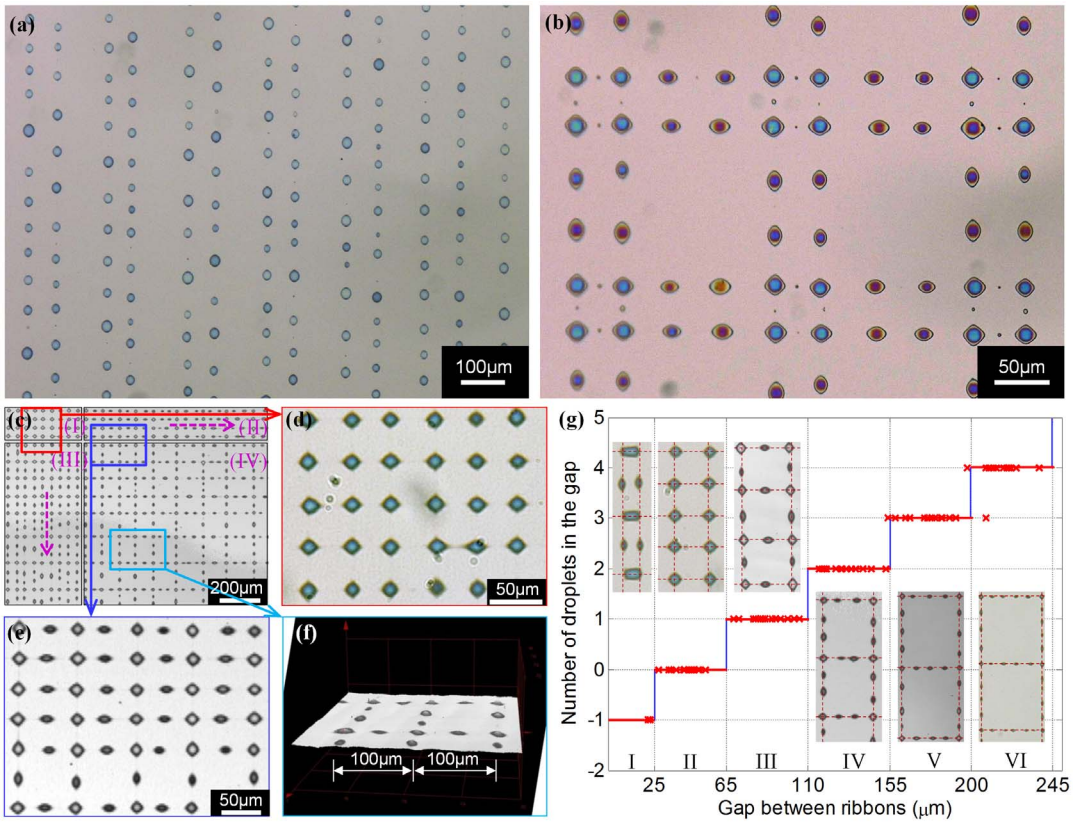

Figure 3 | Large-scale dot-array generated by MDW assisted self-assembly techniques: (a) large-scale dot-array of free self-assembly; (b) large-scale multi-level dot-array of controllable self-assembly based on ribbon-lattice two different diameters; (c) a large-scale dot-array self-assembled out of ribbon-lattices of different periodicity, (d) and (e) are the planar enlarged details, and (f) is the 3-dimensional image of microarray obtained by laser scanning confocal microscope; (g) the relationship between the number of droplets and the gap distance.

rate is 50 nl/min, the applied voltage is 1 kV, and $h_{z\text{-}axis} = 5\ mm$), MDW is unable to deposit linear, aligned microstructures even if the motion stage moves linearly (see Figure 2a). The oscillation is resulted from air turbulence or buckling of solid micro/nanofibers. When $v_{substrate}$ is close to $v_{jetting}$, the "chord" is tightened and the deposited fibers become straight due to the mechanical drawing force. When $v_{substrate}$ exceeds $v_{jetting}$, fiber diameter or ribbon width can be tuned by $v_{substrate}$. Linear arrays of micro/nanofibers with a 50-μm spacing (Figure 2b) are fabricated to demonstrate the relationship between $v_{substrate}$ and micro/nanofibers feature size.

h_{z-axis} also plays an important role in positioning in addition to tuning the degree of solidification. Comparing Figures 2a and 2b, the fibers are written with nozzle-to-substrate distances of 5 mm and 2 mm, respectively. At $h_{z\text{-}axis} = 5\ mm$ (Figure 2a), straight fibers can only be direct-written when $v_{substrate} > v_{jetting}$, whereas the solid fibers will buckle when $v_{substrate} < v_{jetting}$. Inversely, at $h_{z\text{-}axis} = 2\ mm$, the positionability of jetting fiber is free of $v_{substrate}$, and the straight ribbon can be deposited even with very slow speed, such as 50 mm/s, even to 5 mm/s in leap direct-writing discussed behind. The fiber cross-section can continuously tuned by changing applied voltage, substrate speed and nozzle-to-substrate distance (Supplementary Figure S2). It benefits from the *in situ* accumulation of liquid fiber, does not exist the buckling behavior of solid fiber. The speed may improve the uniformity of the ribbon. Additionally, $v_{jetting}$ is a function of $h_{z\text{-}axis}$ that a larger $h_{z\text{-}axis}$ allows longer acceleration time for the jetting fiber under the electric force and the mechanical drawing force.

Fiber diameters are found to vary from 350 nm to 200 nm when $v_{substrate}$ increases from 50 mm/s to 400 mm/s, as shown by zoomed in SEM images in Figure 2c. Figure 2d shows the relationship between the fiber diameter D_{fiber} and the substrate speed $v_{substrate}$ with the fitted relation $D_{fiber} = -0.376 \times 10^{-3}\ V_{substrate} + 0.361$. When $h_{z\text{-}axis}$ increases from 2 mm to 5 mm, the cross-sectional geometry and size of the deposited structures also change. Namely, the fibers become ribbons in the case of small $h_{z\text{-}axis}$, and the width of ribbons is much larger than the diameter of fibers. The main reason is that the liquid fiber spreads on the substrate before it is fully stretched. Figure 2e shows the direct-written ribbon in various speeds of substrate. Figure 2f shows the relationship between the ribbon width D_{fiber} and the substrate speed $v_{substrate}$ with the fitted relation $D_{fiber} = 0.0001V_{substrate}^2 - 0.069V_{substrate} + 16.74$.

The highly aligned micro/nanofibers can be used as a template for the controllable self-assembly of large-scale dot array, in addition to as critical components in flexible energy conversion devices[22], stretchable sensors[23] or as sacrificial structures of nanofabrication[8,24]. Self-assembled dot arrays are widely applicable in microchemical reaction[25], DNA detection[26], and bio-sensing[27], and MDW is a highly robust and relevant method. For instance, in microchemical reaction, one can direct-write different materials in two perpendicular directions. After self-assembly, two materials can form dots at the intersections, to prepare microchemical reaction. The dots can be controlled precisely, and the registration of two materials can be avoided. Further, based on the multi-level dot array, one can easily compare the results before and after microchemical reaction. Free self-assembly has demonstrated the capability to cut fibers into fragments and form dots[28]. Such dynamic behavior is governed by surface tension and Plateau–Rayleigh instability[29,30]. The challenges to transform from free self-assembly to controllable self-assembly are to precisely control the liquid line width, length, and ends, all of which can be addressed by the direct-written ribbon-lattice. A dot array can be direct-written in the following steps. First, MDW is applied to direct-write a parallel array of straight ribbons with uniform width.

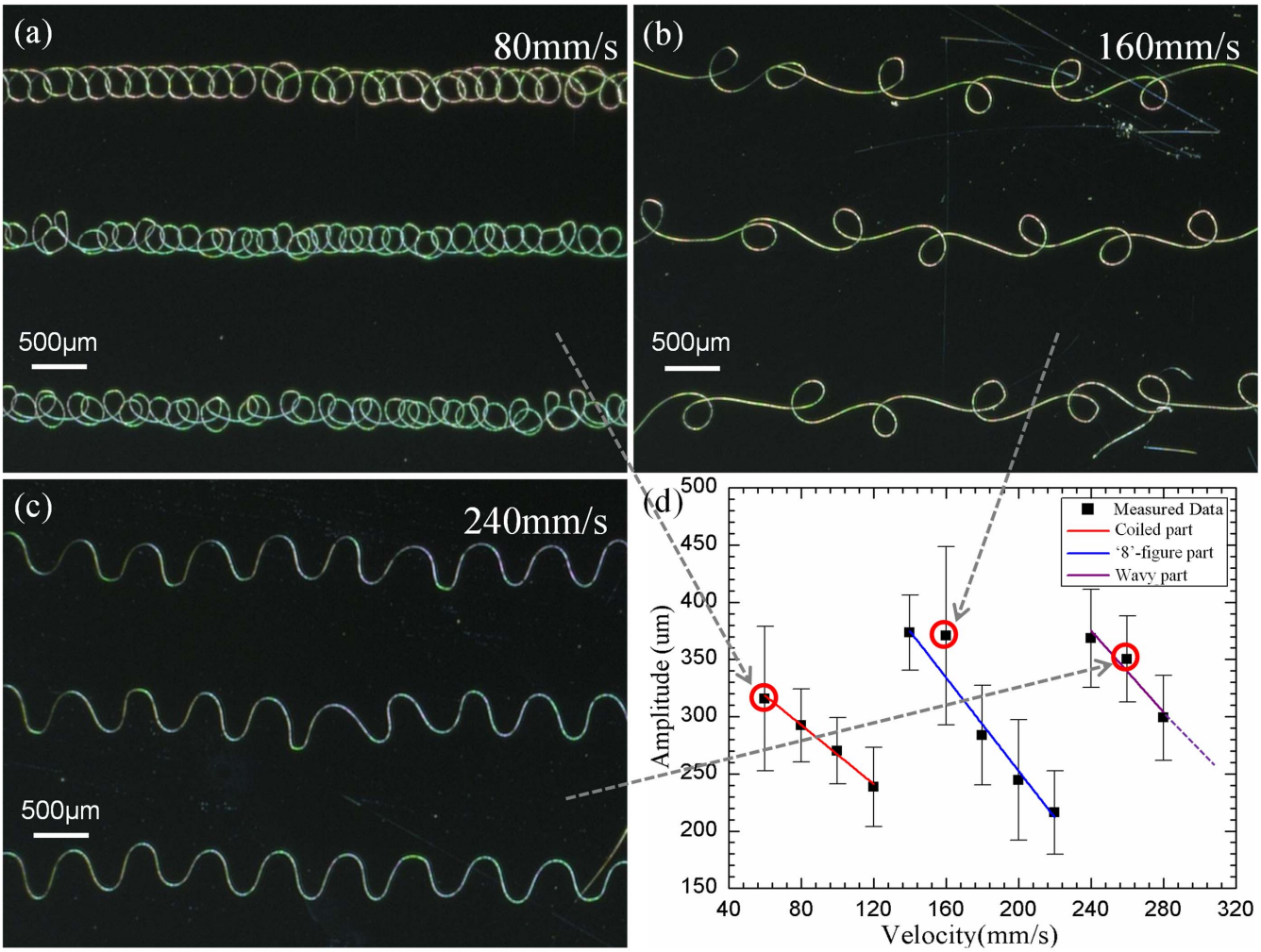

Figure 4 | Single-level serpentine fiber structures: (a) coiled structures; (b) '8'-figure structures; (c) wavy-shaped structures; and (d) relationship between the amplitude of serpentine and the velocity of substrate.

The width is the sole tunable parameter for free self-assembly to control the dot density (supplementary Figure S3). Second, the pattern is placed into a moist environment. As the solid ribbons uptake enough water vapor, it returns liquid, and periodic neckings will appear because the surface instabilities are activated. Finally, the fragmented segments contract longitudinally and grow laterally to form droplets and hence the array of parallel ribbons self-assemble into an array of small dots as the solvent continues evaporating. Therefore the three key steps of the self-assembly include necking, fragmenting, and contracting. Figure 3a shows a large-scale dot-array formed from straight parallel fibers in free self-assembly, and Figure 3b shows the controllable self-assembly of multi-level dot-array. Dot arrays self-assembled out of ribbon lattices with different width and gap (Figure 3c–f), to show that the finer the fibers are, the higher the density is. Figure 3g shows that there exists an obvious relationship between the number of droplets and the ribbon gap. In *Region I* there is no necking and two nearest intersections merge into one dot. It suggests that the ribbon lattices are unable to self-assemble when the lattice periodicity is smaller than 25 μm for $b_{ribbon} \approx$ 10.7 μm. In *Region II*, the dots are exactly located at the intersections of the ribbon lattice. Highly ordered and uniform microarrays can be fabricated, meanwhile the dot array periodicity can be continuously tuned from 25 μm to 65 μm. In *Region III*, there is one intermediate dot in each gap, indicating hierarchical microdot arrays can be generated. The dot array periodicity can be determined by halving the lattice periodicity (65/2 μm = 32.5 μm, 110/2 μm = 55 μm). When the ribbon lattice periodicity is larger than 65 μm, a new droplet will be added every 45 μm. The dot size and position are dominated by the lattices, so an arbitrary dot-array can be self-assembled in a controllable manner.

Helix direct-writing of serpentine structures. Serpentine structures are widely used in stretchable electronics to enhance the stretchability[31] and reduce the stiffness[32] of stiff electronic materials. Helix direct-writing can write serpentine structures in direct, continuous and controllable manners when 15 $mm < h_{z\text{-axis}} < 45$ mm. The ink often exhibits complex dynamics, such as the 'whipping/buckling' instability so that the ink "dances" at a distance not far from the motion stage, $h_{whipping}$, as shown in Fig. 1a[4,33,34]. The first occurrence of non-axisymmetric instability locates at $h_{straight} < h_{z\text{-}axis} < h_{straight} + h_{whipping}$. We take advantage of the instability to direct-write serpentine structures by linear translation of the motion stage (see supplementary Figure S4). When 15 $mm < h_{z\text{-axis}} < 45$ mm, the unstable 'whipping/buckling' behavior is able to be controlled, and the unstable jet fiber can be positioned on the substrate by the combined control of substrate speed and nozzle-to-substrate distance, and applied voltage. Complex microstructures we have successfully written are coils (Figure 4a), "8"-shaped "vines" (Figure 4b), and sinuous (Figure 4c). The former two microstructures, except the sinuous microstructures, can also be direct-written by melt electrospinning[35]. However the sinuous microstructures is more important in enhancing the deformability of stretchable electronics.

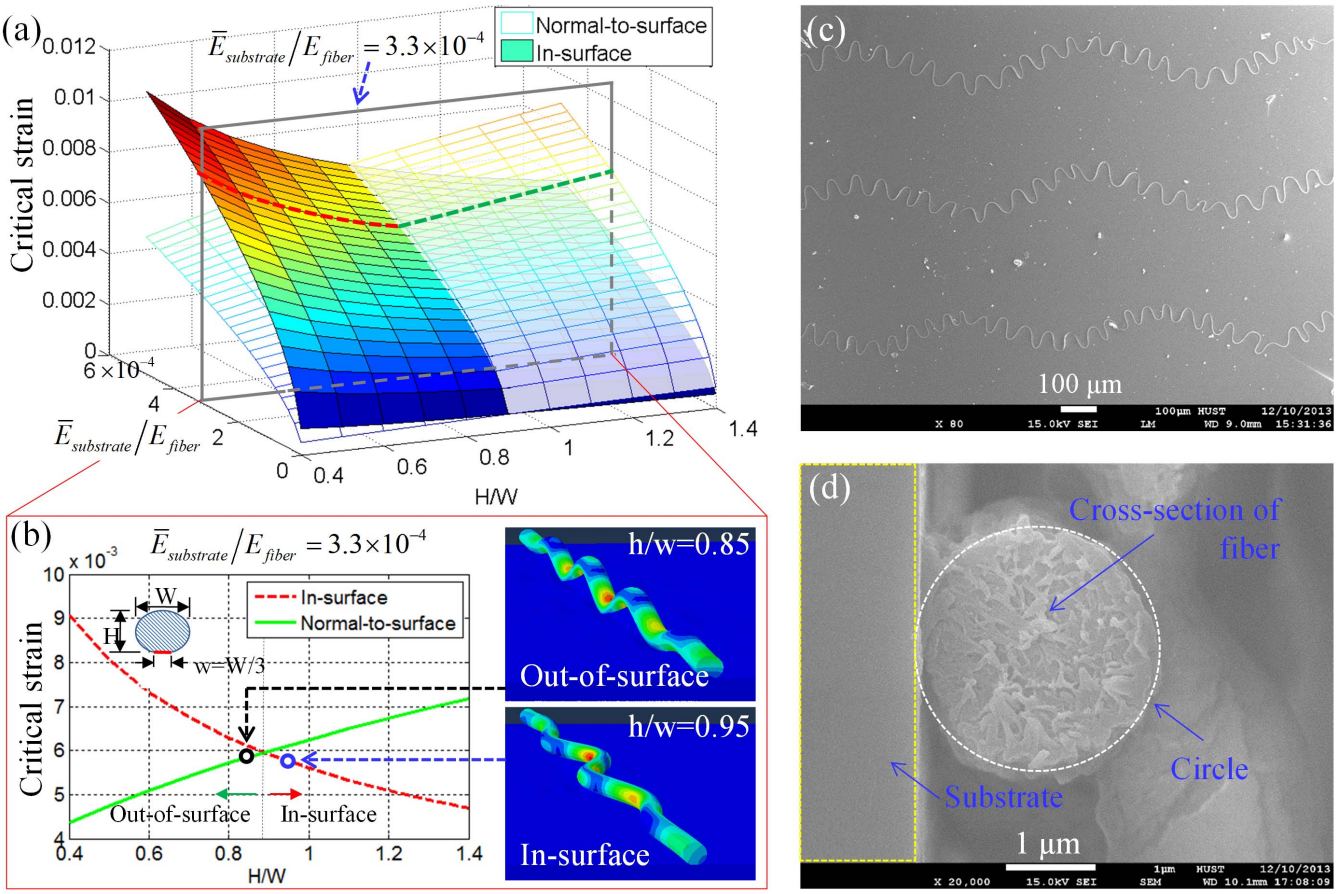

Figure 5 | Critical strain for in-surface buckling and out-of-surface buckling. (a) The semi-elliptical cross-section's critical strain for both in-plane and out-of-plane buckling. (b) The specific is $\bar{E}_{substrate}/E_{fiber} = 3.3 \times 10^{-4}$, and the finite element simulation of in-surface and out-of-surface buckling. (c) The SEM figure of self-similar serpentine structures. (d) The circular cross-section of the self-similar structures.

The $v_{substrate}$ can digitally control the layout of deposited fibers, from coils to serpentines, to straight lines, with the increase of $v_{substrate}$, as shown in Figure 4. When $v_{substrate} > v_{jetting}$, HDW converts to MDW, with less control of position due to the larger nozzle-to-substrate distance. In experiment (the solution is PVDF (Polyvinylidene fluoride) with 16% concentration (Dimethylformamide: acetone = 6 : 4), and $U_{applied}$ = 2.2 *kV*, h_{z-axis} = 25 *mm*, Q_{flow}= 600 *nl*/min), three critical speeds are observed to divide the patterns into four kinds of shapes: coiled, "8"-shaped, serpentine and straight structures, where the transition speeds are about 130 mm/s, 230 mm/s and 330 mm/s. Thus, it indicates that the breaking point between the meandering and straight patterns is the onset of the fiber buckling. The structural period linearly decreases with $v_{substrate}$. Due to small substrate speed, the fiber is only stretched by electrical field, and the mechanical drawing force only plays a guiding role in positioning the fibers along the motion direction. The shape of deposited structure is determined by the relative velocity and the instability of jetting, when other processing parameters are fixed.

The $U_{voltage}$ plays a critical and complex role in controlling the dynamic behavior of electrospinning. It may influence the jetting speed $v_{jetting}$, fiber diameter and stable length $h_{straight}$ simultaneously (Figure 1a). A series of experiments were carried out, where h_{z-axis} = 25 *mm*, and $U_{voltage}$ from 1.7 kV to 3.3 kV with the incremental interval of 0.2 kV. The jetting speed increases monotonically with the applied voltage. It can be observed at the speed of 200 mm/s that only straight fibers can be deposited on the substrate at 1.7 kV, whereas serpentine fibers are deposited at 1.9 kV. That is to say the jetting speed exceeds the substrate speed, namely $v_{jetting} > v_{substrate}$, when $U_{voltage}$ increases from 1.7 kV to 1.9 kV. On the other hand, the rotation speed of helix motion also progressively increases with $U_{voltage}$. It explains that only coiled fibers can be deposited when $U_{voltage} \geq 2.1$ *kV*, and the space of coiled fibers decreases monotonically with $U_{voltage}$.

The h_{z-axis} serves two critical purposes. One role is to differentiate HDW (for complex curvy fibers) from MDW (for straight fibers). When $h_{z-axis} < h_{straight}$, HDW decays back to MDW. The other role of h_{z-axis} is to determine the radius of the conical helix of whipping segment, to control the serpentine amplitude and wavelength. The rotation radius at the bottom increases monotonically with h_{z-axis}. Serpentine structure with large amplitude and small wavelength can be formed by digitally tuning h_{z-axis} and $v_{substrate}$, to improve the stretchability of electronic devices. Furthermore, the ratio of amplitude and wavelength can be increased by depositing fiber onto uniaxially prestrained substrate.

We adopt HDW to fabricate self-similar serpentine structures that are used in stretchable devices. The self-similar serpentine structures will increase the stretchability significantly, and are useful for stretchable electronic devices which are composed of large areas of undeformable components, especially avoiding out-of-surface deformation at stretching[36–38]. This process contains three main steps (supplementary Figure S5): 1) HDW direct-writes the first-level serpentine structures on Si substrate; 2) the transfer printing is utilized to transfer the serpentine structures from Si substrate to a prestrained rubber substrate; and 3) the buckling of serpentine structures occurs to form the hierarchical buckling structures, when the prestrained substrate is released from the prestrain $\varepsilon_{prestrain}$, which has to be larger than the critical buckling strain. Two different buckling modes are observed in experiments: in-surface buckling and out-of-surface

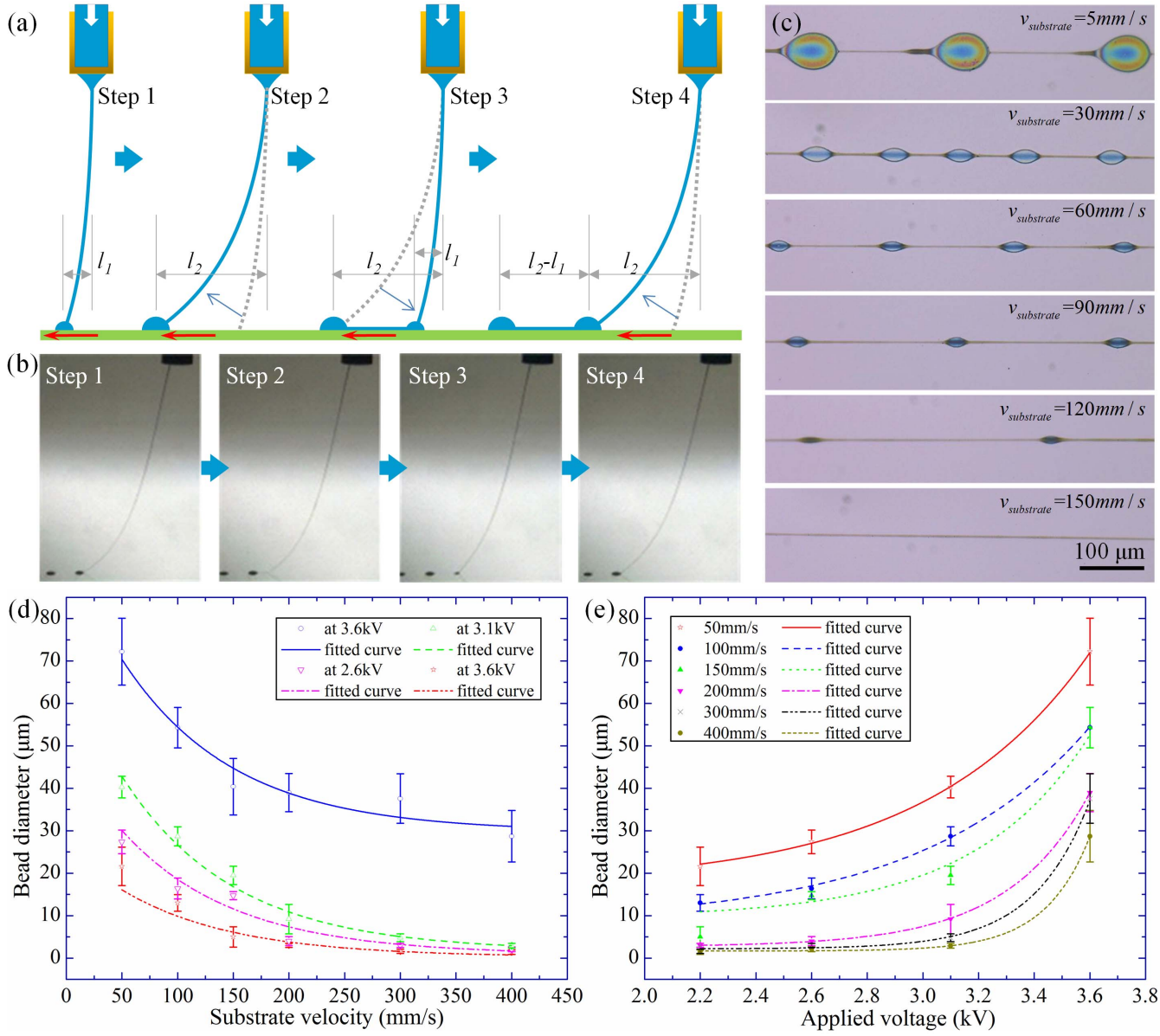

Figure 6 | The leap direct-writing technique: (a) the schematic diagram of leap direct-writing: the ink first accumulates at contact point and then gets stretched by mechanical drawing force. At a critical distance, the ink leaps to the next contact point, and gets stretched again; (b) the leap direct-writing is captured by high-speed camera, similar with (a); and (c) different structures are deposited in the condition of applied voltage (1 kV), nozzle-to-substrate distance (2 mm), flow rate (50 nl/min). (d) and (e) show the effects of substrate speed and voltage on bead diameter. (d) The color lines are fitting curves at different applied voltage. The error bars present the standard deviation to the average values of 10 measurement results. (e) The color lines are fitting curves at different substrate speed. Supply rate, nozzle-to-substrate distance and nozzle diameter are 1200 nl/min, 7.5 mm and 145 μm, respectively.

buckling. We have confirmed the critical conditions for in- and out-of-surface buckling theoretically and experimentally[23]. The critical strains for in- and out-of-surface buckling are related to the fiber cross-section and the Young's moduli of the fiber and the rubber substrate. The critical strains for in-surface and out-of-surface buckling modes are $\varepsilon_{in-sruface} \approx \sqrt{\frac{\bar{E}_{substrate}}{E_{fiber}}} \times \frac{\sqrt{I_{in-surface}}}{A}\left(\frac{1}{2}+2\pi\Big/(5-2\gamma-2\ln\frac{5}{7}-\frac{1}{2}\ln\frac{w^4}{16}\frac{\bar{E}_{substrate}}{E_{fiber}I_{in-surface}})\right)$ and $\varepsilon_{out-surface} \approx \sqrt{\frac{\bar{E}_{substrate}}{E_{fiber}}} \times \frac{\sqrt{I_{out-surface}}}{A}\left(\frac{9}{16}+\frac{16\pi}{9}\Big/(3-2\gamma-2\ln\frac{3}{4}-\frac{1}{2}\ln\frac{w^4}{16}\frac{\bar{E}_{substrate}}{E_{fiber}I_{out-surface}})\right)$, respectively, where $I_{in-surface}$ and $I_{out-surface}$ are the moment of inertia of the fiber along the in-surface and normal-to-surface directions. The buckling mode can be predicated comparing $\varepsilon_{prestrain}$ with the critical strains of in-/out-of-surface buckling. When $\varepsilon_{prestrain} < \min(\varepsilon_{out-surface}, \varepsilon_{in-surface})$, the fiber gets compressed without any buckling. If $\varepsilon_{prestrain} < \min(\varepsilon_{out-surface}, \varepsilon_{in-surface})$, the in-surface buckling occurs when $\varepsilon_{out-surface} > \varepsilon_{in-surface}$, and the out-of-surface buckling occurs when $\varepsilon_{out-surface} > \varepsilon_{in-surface}$.

Figure 5 shows the critical strains for in- and out-of-surface buckling of deposited fibers with elliptical cross-section. The Young's modulus ratio has a significant effect on the critical strains of each buckling mode, but very little contribution to in- and out-of-surface buckling mode transformation. The critical point is mainly determined by the cross-section of deposited fiber. Figure 5b is the case that the Young's modulus ratio $\bar{E}_{substrate}/E_{fiber} = 3.3 \times 10^{-4}$, and we get the critical point is $H/W \approx 0.9$. The right of Figure 5b is the finite element simulation of the buckling mode for different elliptical cross-

sections. Figure 5c is an SEM figure of self-similar serpentine structure with hierarchical serpentine structures, and more can be seen in supplementary Figure S6. The cross-section is close to a circle (Figure 5d), which guarantees in-surface buckling of the first-order serpentine structures.

Leap direct-writing of bead-on-string structures. Leap direct-writing can digitally deposit the bead-on-string structures when $0.5\ mm < h_{z\text{-axis}} \leq 2\ mm$ and $v_{substrate} \leq 120\ mm/s$, as schematically shown in Figure 6a. There are four key steps involved in LDW. In *Step 1*, the ink is jetted from the attached Taylor cone, and a fiber links the nozzle and substrate. When $h_{z\text{-axis}} = 2\ mm$, the fiber remains liquid when reaching the substrate. The liquid fiber accumulates at the contact point, forming a big drop if the substrate stays quiescent, in a sense similar with aerial refueling. In *Step 2*, when the substrate starts to move slowly, the jet fiber will gradually slope to match the substrate speed. In *Step 3*, the jet fiber jumps to the next point at a critical distance (at the speed of <120 mm/s), and the next identical cycle begins in *Step* 4. The formation of bead-on-string microstructures is composed of anchoring of contact point, stretching of liquid jet fiber, and skipping to the next contact point. The corresponding experimental steps are captured by high-speed camera (Figure 6b). These phenomena are mainly resulted from the competition of the viscoelastic strength of jet fiber with the combination of mechanical drawing force and electrical field force[39]. The manufacturing mechanism is intrinsically different from free self-assembly which demonstrates weaker control in positioning[40].

The substrate speed controls the bead size and the string length, when $h_{z\text{-axis}}$ and $U_{voltage}$ are fixed. The accumulation time for the bead gets shorter with higher substrate speed, so that the bead diameter gradually decreases to the line width, and the string becomes longer and longer when the substrate speed reaches that of line writing. Additionally, the mechanical drawing force applied on the liquid fiber increases as the viscosity of the polymer solution enhances. Different bead-on-string structures obtained when varying substrate speeds from 5 mm/s to 120 mm/s are shown in Figure 6c, with the flow rate of 50 nl/min and $U_{voltage} = 1.25\ kV$. The beads are large at slow speed, and completely disappear when the speed reaches >150 mm/s. To further control the size of each bead, the substrate speed should be programmed to tune the time for 'aerial refueling'. We also fabricate arrays of silicon nozzles to direct-write bead-on-string structures[41]. The microstructures are captured by confocal laser scanning microscopy (Supplementary FigureS7), with $U_{voltage} = 2.2\ kV$ fixed. Fine fibers can be written when substrate speed is 400 mm/s, $h_{z\text{-axis}} = 7.5\ mm$, and flow rate is 1200 nl/min. It indicates that the silicon nozzle array is suitable for large-scale printing of bead-on-string structures. The experiment results show that the critical speed $v_{critical}$ to transform from bead-on-string mode to fiber mode is between 150 mm/s and 200 mm/s. Figure 6d shows the bead size changes with the substrate speed at different applied voltage. When $v_{substrate} < v_{critical}$, bead-on-string microstructures are fabricated. When $v_{substrate} < v_{critical}$, the accumulation effect disappears, and LDW decays into MDW, where the fiber will be continuously pulled by the mechanical drawing force, and only line structures are fabricated.

Figure 6e shows that the applied voltage can also tune the size of bead-on-string structures. Si-nozzle was adopted to study the dependence, and four groups of experiments were carried out: 3.6 kV, 3.1 kV, 2.6 kV, and 2.2 kV, where the flow rate and nozzle-to-substrate distance kept constant (6 wt% PEO at 1200 nl/min, $h_{z\text{-axis}} = 7.5$ mm). In each experiment, the substrate speed $v_{substrate}$ changes from 50 mm/s to 400 mm/s. It can be found that the bead enlarges monotonically with applied voltage at a constant substrate speed. It can also be noted that the critical voltage for the spurt of bead size growth is located between 3.1 kV and 3.6 kV.

Conclusion

A versatile MES direct-writing technique that can directly write high-viscosity ink on flexible substrates, in a continuous, high-resolution, noncontact, and low-temperature manner is developed to fabricate micro/nano-structures of various morphology and resolution by digitally tuning three key processing parameters: the substrate speed, the nozzle-to-substrate distance, and the applied voltage. The mechanical drawing force controlled by the substrate speed plays a critical role in the improvements over NFES techniques in terms of the resolution, positioning, and alignment of micro/nanofibers. The various micro/nano-structures will serve as the building blocks of a flexible or stretchable electronics. Arrayed structures can potentially be written simultaneously by multiply nozzles, which represents a viable solution for high-throughput manufacture using MES.

1. Li, Y., Fu, Z.-Y. & Su, B.-L. Hierarchically Structured Porous Materials for Energy Conversion and Storage. *Adv. Funct. Mater.* **22**, 4634–4667 (2012).
2. Yang, H. F., Lightner, C. R. & Dong, L. Light-Emitting Coaxial Nanofibers. *Acs Nano* **6**, 622–628 (2012).
3. Gumennik, A. *et al.* All-in-Fiber Chemical Sensing. *Adv. Mater.* **24**, 6005–6009 (2012).
4. Huang, Y. *et al.* Electrohydrodynamic direct-writing. *Nanoscale* **5**, 12007–12017 (2013).
5. Sun, D., Chang, C., Li, S. & Lin, L. Near-Field Electrospinning. *Nano Lett.* **6**, 839–842 (2006).
6. Chang, C., Limkrailassiri, K. & Lin, L. W. Continuous near-field electrospinning for large area deposition of orderly nanofiber patterns. *Appl. Phys. Lett.* **93**, 123111 (2008).
7. Wang, X. *et al.* Fabrication of nanochannels via near-field electrospinning. *Appl. Phys. A-mater.* **108**, 825–828 (2012).
8. Min, S. Y. *et al.* Large-scale organic nanowire lithography and electronics. *Nat. Commun.* **4**, 1773 (2013).
9. Agarwal, S., Greiner, A. & Wendorff, J. H. Electrospinning of Manmade and Biopolymer Nanofibers-Progress in Techniques, Materials, and Applications. *Adv. Funct. Mater.* **19**, 2863–2879 (2009).
10. Yin, Z. P., Huang, Y. A., Bu, N. B., Wang, X. M. & Xiong, Y. L. Inkjet printing for flexible electronics: Materials, processes and equipments. *Chin. Sci. Bull.* **55**, 3383–3407 (2010).
11. Calvert, P. Inkjet printing for materials and devices. *Chem. Mater.* **13**, 3299–3305 (2001).
12. Chung, S. *et al.* Inkjet-printed stretchable silver electrode on wave structured elastomeric substrate. *Appl. Phys. Lett.* **98**, 153110 (2011).
13. Sirringhaus, H. *et al.* High-resolution inkjet printing of all-polymer transistor circuits. *Science* **290**, 2123–2126 (2000).
14. Yun, Y. H. *et al.* A Glucose Sensor Fabricated by Piezoelectric Inkjet Printing of Conducting Polymers and Bienzymes. *Anal. Sci.* **27**, 375–379 (2011).
15. Jung, H. C., Cho, S. H., Joung, J. W. & Oh, Y. S. Studies on inkjet-printed conducting lines for electronic devices. *J. Electron. Mater.* **36**, 1211–1218 (2007).
16. Forrest, S. R. The path to ubiquitous and low-cost organic electronic appliances on plastic. *Nature* **428**, 911–918 (2004).
17. Park, J. U. *et al.* High-resolution electrohydrodynamic jet printing. *Nat. Mater.* **6**, 782–789 (2007).
18. de Gans, B. J., Duineveld, P. C. & Schubert, U. S. Inkjet Printing of Polymers: State of the Art and Future Developments. *Adv. Mater.* **16**, 203–213 (2004).
19. Li, D., Ouyang, G., McCann, J. T. & Xia, Y. N. Collecting electrospun nanofibers with patterned electrodes. *Nano Lett.* **5**, 913–916 (2005).
20. Li, D. & Xia, Y. Electrospinning of nanofibers: Reinventing the wheel? *Adv. Mater.* **16**, 1151–1170 (2004).
21. Greiner, A. & Wendorff, J. H. Electrospinning: A fascinating method for the preparation of ultrathin fibres. *Angew. Chem. Int. Ed.* **46**, 5670–5703 (2007).
22. Chang, C. E., Tran, V. H., Wang, J. B., Fuh, Y. K. & Lin, L. W. Direct-Write Piezoelectric Polymeric Nanogenerator with High Energy Conversion Efficiency. *Nano Lett.* **10**, 726–731 (2010).
23. Duan, Y., Huang, Y., Yin, Z., Bu, N. & Dong, W. Non-wrinkled, highly stretchable piezoelectric devices by electrohydrodynamic direct-writing. *Nanoscale* **6**, 3289–3295 (2014).
24. Khudiyev, T., Huseyinoglu, E. & Bayindir, M. Non-resonant Mie scattering: emergent optical properties of core-shell polymer nanowires. *Sci. Rep.* **4**, 4607 (2014).
25. Xu, B. B., Zhang, Y. L., Wei, S., Ding, H. & Sun, H. B. On-Chip Catalytic Microreactors for Modern Catalysis Research. *Chemcatchem* **5**, 2091–2099 (2013).
26. Shigeta, K. *et al.* Functional Protein Microarrays by Electrohydrodynamic Jet Printing. *Anal. Chem.* **84**, 10012–10018 (2012).
27. Arrabito, G. & Pignataro, B. Solution Processed Micro- and Nano-Bioarrays for Multiplexed Biosensing. *Anal. Chem.* **84**, 5450–5462 (2012).

28. Huang, Y., Wang, X., Duan, Y., Bu, N. & Yin, Z. Controllable self-organization of colloid microarrays based on finite length effects of electrospun ribbons. *Soft Matter* **8**, 8302–8311 (2012).
29. Brochardwyart, F. & Redon, C. Dynamics of Liquid Rim Instabilities. *Langmuir* **8**, 2324–2329 (1992).
30. Kondic, L., Diez, J. A., Rack, P. D., Guan, Y. F. & Fowlkes, J. D. Nanoparticle assembly via the dewetting of patterned thin metal lines: Understanding the instability mechanisms. *Phys. Rev. E* **79**, 026302 (2009).
31. Kim, D. H. *et al.* Materials and noncoplanar mesh designs for integrated circuits with linear elastic responses to extreme mechanical deformations. *Proc. Natl. Acad. Sci.* **105**, 18675–18680 (2008).
32. Kim, D. H. *et al.* Epidermal Electronics. *Science* **333**, 838–843 (2011).
33. Duan, Y., Huang, Y. & Yin, Z. Transfer printing and patterning of stretchable electrospun film. *Thin Solid Films* **544**, 152–156 (2013).
34. Huang, Z. M., Zhang, Y. Z., Kotaki, M. & Ramakrishna, S. A review on polymer nanofibers by electrospinning and their applications in nanocomposites. *Compos. Sci. Technol.* **63**, 2223–2253 (2003).
35. Brown, T. D., Dalton, P. D. & Hutmacher, D. W. Direct Writing By Way of Melt Electrospinning. *Adv. Mater.* **23**, 5651–5657 (2011).
36. Su, Y. *et al.* Postbuckling analysis and its application to stretchable electronics. *J. Mech. Phys. Solids* **60**, 487–508 (2012).
37. Fan, J. A. *et al.* Fractal design concepts for stretchable electronics. *Nat. Commun.* **5**, 3266 (2014).
38. Xu, S. *et al.* Stretchable batteries with self-similar serpentine interconnects and integrated wireless recharging systems. *Nat. Commun.* **4**, 1543 (2013).
39. Bu, N. B., Huang, Y. A., Deng, H. X. & Yin, Z. P. Tunable bead-on-string microstructures fabricated by mechano-electrospinning. *J. Phys. D. Appl. Phys.* **45**, 405301 (2012).
40. Tian, X. L., Bai, H., Zheng, Y. M. & Jiang, L. Bio-inspired Heterostructured Bead-on-String Fibers That Respond to Environmental Wetting. *Adv. Funct. Mater.* **21**, 1398–1402 (2011).
41. Pan, Y. Q., Huang, Y. A., Bu, N. B. & Yin, Z. P. Fabrication of Si-nozzles for parallel mechano-electrospinning direct writing. *J. Phys. D. Appl. Phys.* **46**, 255301 (2013).

Acknowledgments

The authors acknowledge supports from the National Natural Science Foundation of China (51322507, 51175209, 51121002) and the Fundamental Research Funds for the Central Universities (2013TS019). The general characterization facilities were provided through the National Laboratory.

Author contributions

Y.A.H. and Z.P.Y. designed the experiments and wrote the manuscript. Y.A.H., Y.Q.D. and Y.J.D. performed the direct-writing experiments. Y.A.H., N.B.B., Y.Q.P. and N.S.L. analyzed the data, and discussed the results. All authors reviewed the manuscript.

Additional information

Supplementary information accompanies this paper at http://www.nature.com/scientificreports

Competing financial interests: The authors declare no competing financial interests.

How to cite this article: Huang, Y. *et al.* Versatile, kinetically controlled, high precision electrohydrodynamic writing of micro/nanofibers. *Sci. Rep.* **4**, 5949; DOI:10.1038/srep05949 (2014).

Supplementary Information

Versatile, kinetically controlled, high precision electrohydrodynamic writing of micro/nanofibers

YongAn Huang[1,*], Yongqing Duan[1], Yajiang Ding[1], Ningbin Bu[1], Yanqiao Pan[1], Nanshu Lu[2], Zhouping Yin[1,*]

[1]State Key Laboratory of Digital Manufacturing Equipment and Technology, Huazhong University of Science and Technology, Wuhan, 430074, China

[2]Center for Mechanics of Solids, Structures and Materials, Department of Aerospace Engineering and Engineering Mechanics, University of Texas at Austin, Austin, Texas 78712, USA

[*] Corresponding author: Y.A. Huang, yahuang@hust.edu.cn, Z.P. Yin, yinzhp@mail.hust.edu.cn.

1. The fiber slope controlled by the substrate speed

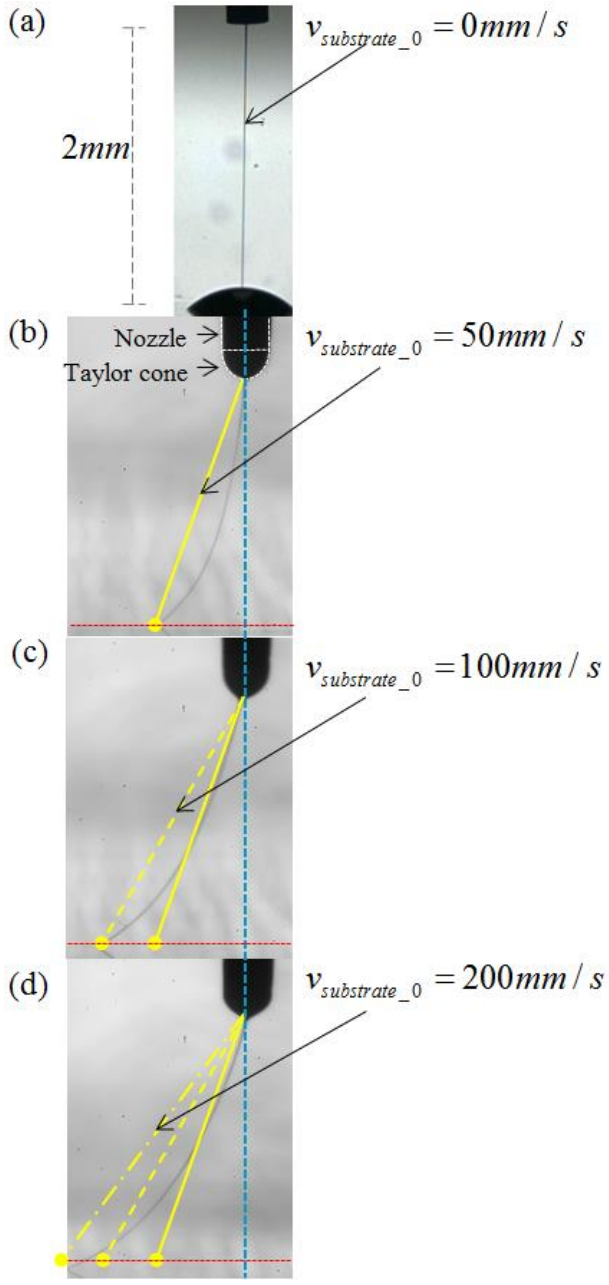

Supplementary Figure S1. The effect of substrate speed on the slope of fiber, captured by high-speed camera. (a) The fibre is jetted when the motion stage is stationary. (b)-(d) denote the jet when the velocity of motion stage is 50 mm/s, 100 mm/s and 200 mm/s, respectively. The voltage is 0.8 kV, the distance is 2 mm, and the flow rate is 50 nl/min. The degree of slant θ is increased with the speed, so the trajectory planning varies with the velocity. The drawing force and elongation rate increase rapidly for the high moving speed. The high-speed camera is utilized to determine the trigger voltage to generate jet flow and the lowest voltage to stable the Taylor cone.

2. Continuously tunable cross-section of electrospun fiber

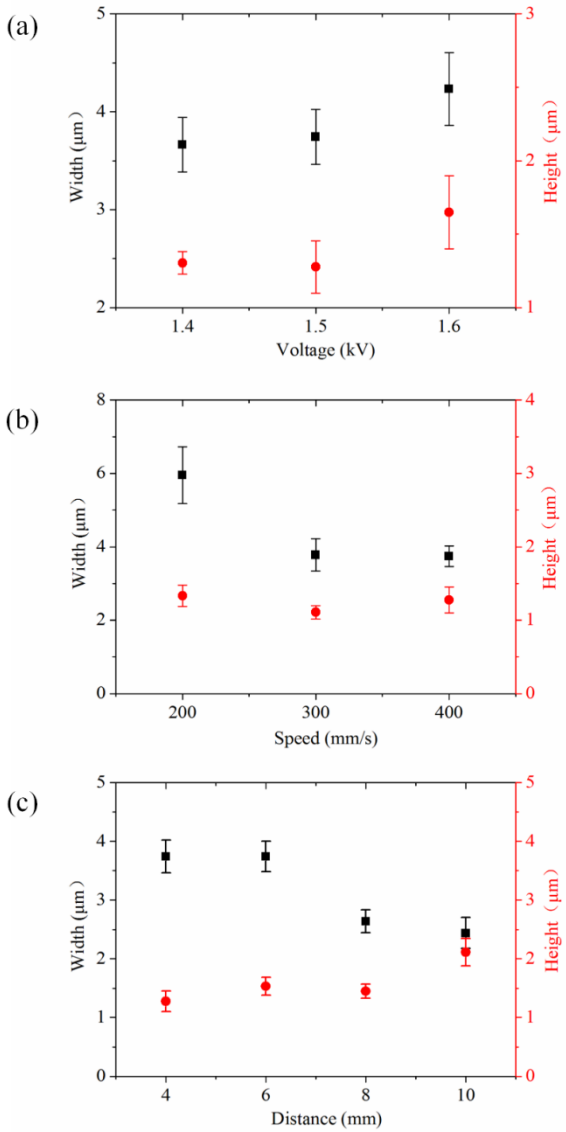

Supplementary Figure S2. Electrospun fiber's width and height vs applied voltage, substrate speed and nozzle-to-substrate distance. (a) It shows the width and height related with the applied voltage, where the distance is 4 mm and the speed is 400 mm/s. The width and height all increase monotonously with the applied voltage. (b) It shows the width and height related with the substrate speed, where the distance is 4 mm and the voltage is 1.5 kV. The width and height all decrease monotonously with the substrate speed. (c). It shows the width and height related with the nozzle-to-substrate distance, where the voltage is 1.5 kV, and the speed is 400 mm/s. The width decreases monotonously with the nozzle-to-substrate distance. However, the height increases monotonously with the nozzle-to-substrate distance. So the aspect ratio can be tuned by the

nozzle-to-substrate distance.

3. Controllable self-assembly based on direct-written fiber structures

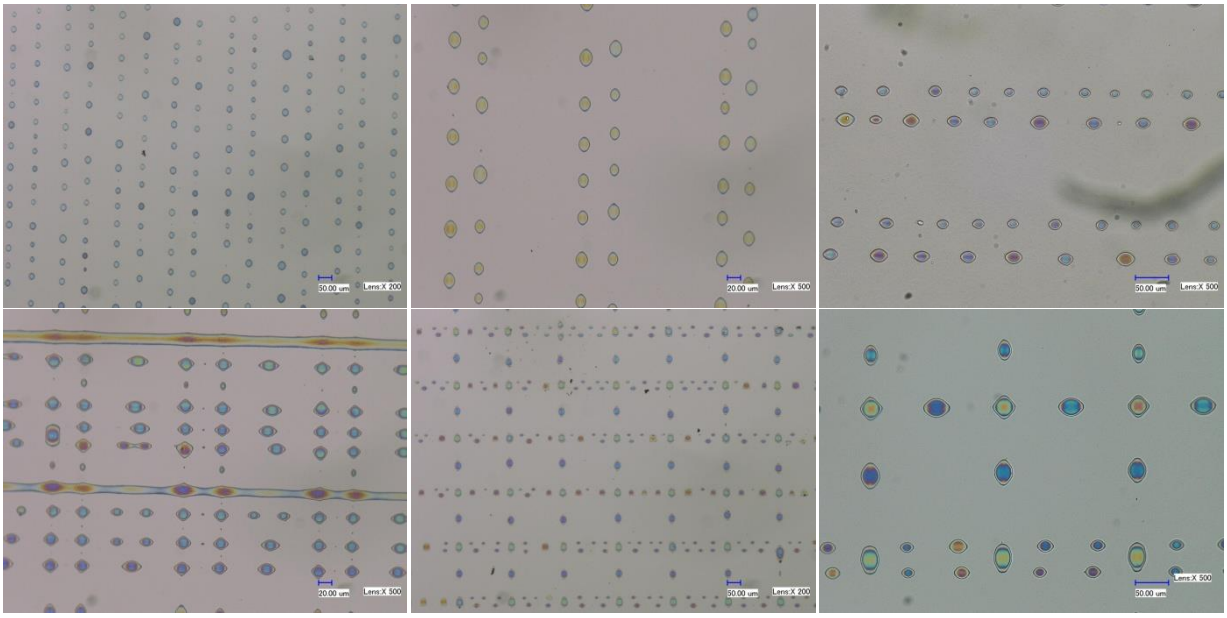

Supplementary Figure S3. Large scale dot array self-assembly using MDW direct-writing. (a) Large scale dot-array with uniform diameter and gap is formed by straight parallel fiber array with the same diameter and the same gap between fibers; (b) Large scale dot-array with uniform diameter and different gap is resulted from straight fiber array with the same diameter and the different gaps between fibers; (c) Dot array with different diameter and gap are generated by straight fiber array with different diameters and gaps; (d) The effect of fiber diameter on formation velocity that coarse structures need more time to realize self-assembly; Further to improve the regularity of the dot array, one can fabricate fiber grid. If the gap between fibers is small enough or the diameter is large enough, the dots just appear at the intersection. Otherwise, there will appear dot between intersections. (e)The effect of fiber diameter on density of dot; In order to show the effect of gap and diameter, the fiber grid with different diameter and gap is fabricated. The finer the fibers are, the more the dot generated between intersections. (f) Detail with enlarged scale.

4. Helix direct-writing for serpentine structures

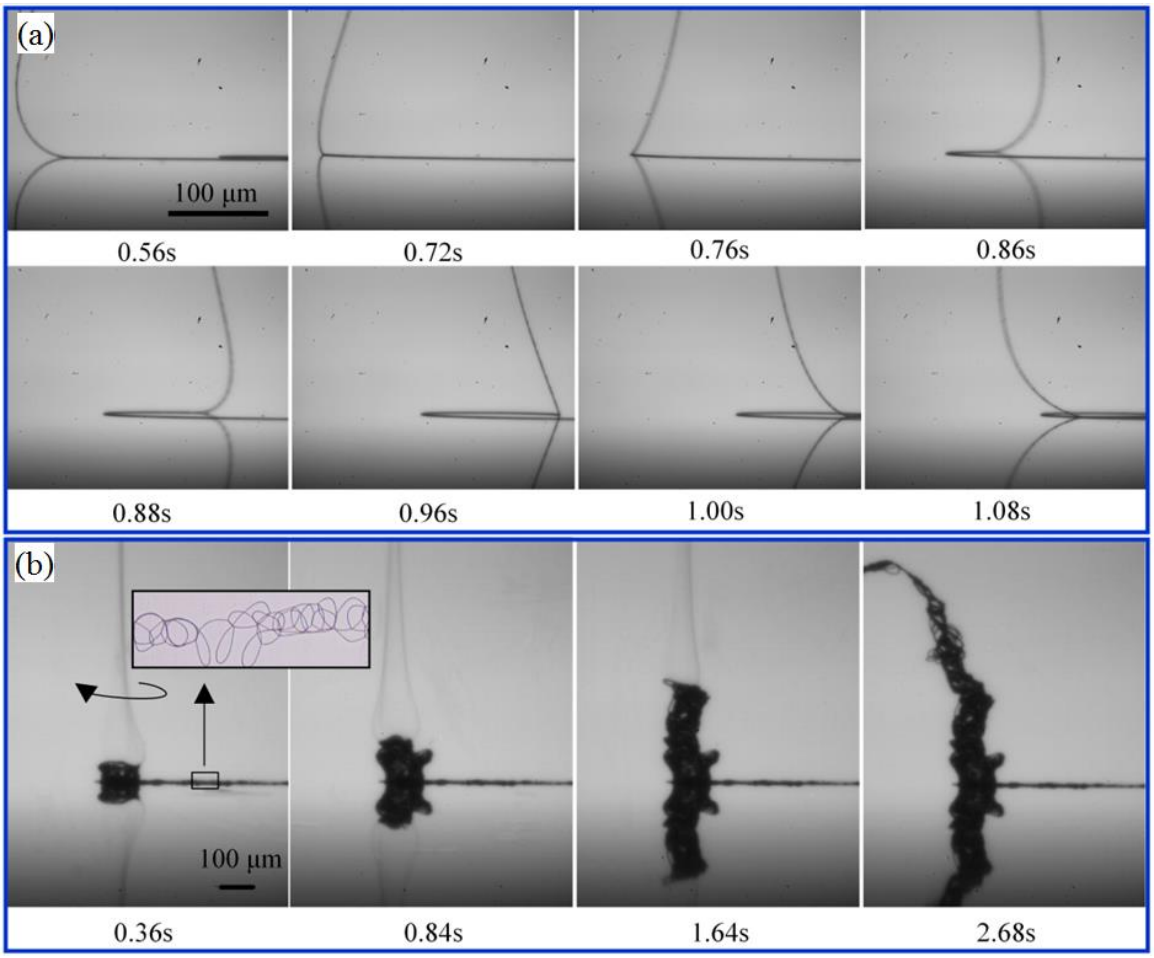

Supplementary Figure S4. Different jet state in the different velocity mode of the substrate. (a) Buckling of the jet when the substrates is accelerated to 5 cm/s. The jet is compressed to buckling and then rotates along the nozzle axis with a stable cycle. However, the rotation is not completed one circle due to this high velocity of the substrate. The transverse swing induces zigzag patterns. (b) Spiral jet deposits in the upward direction cycle-by-cycle on the static substrate. More regular meandering fiber patterns can be obtained by lower velocity. After the velocity overpasses 100 mm/s, the jet comes into the stable curvilinear motion mode with catenary shape due to pulling force. The experiment condition is the volume flow rate Q=100 nl/min, the applied voltage U=1.5 kV, the nozzle-to-substrate distance H=0.5 cm and the substrate is silicon.

.

5. The fabrication of self-similar serpentine structures

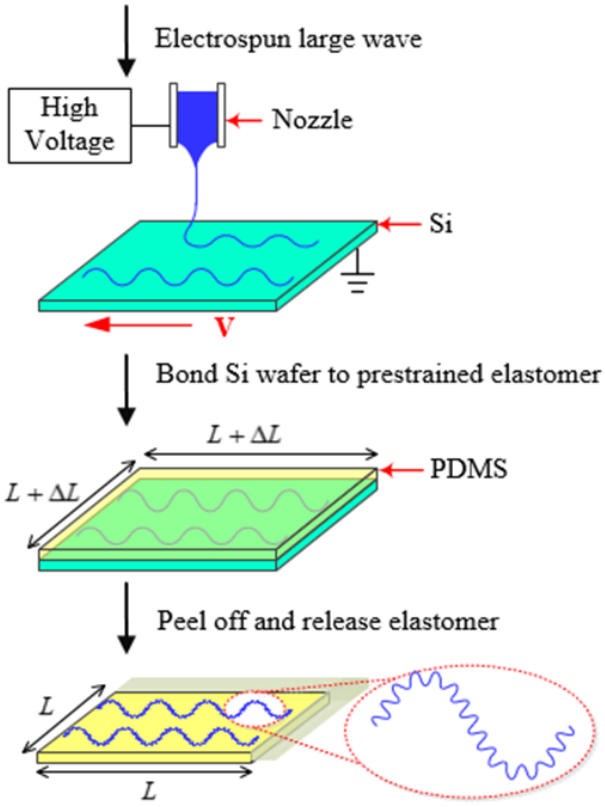

Supplementary Figure S5. Schematic of fabrication of self-similar serpentine structures. 1) The first-level wavy structure is direct-written on Si substrate based on the whipping effect, usually considered as a kind of unstability. 2) Si wafer with the first-level wavy structure is pressed onto a prestrained elastomer with the top surface of Si wafer. The wavy structure is transferred onto the elastomer because of the large viscoelasticity of elastomer. 3) The prestrained substrate is released, and the self-similar structure is formed due to the self-organized buckling behavior when the prestrain is larger than the critical strain of buckling.

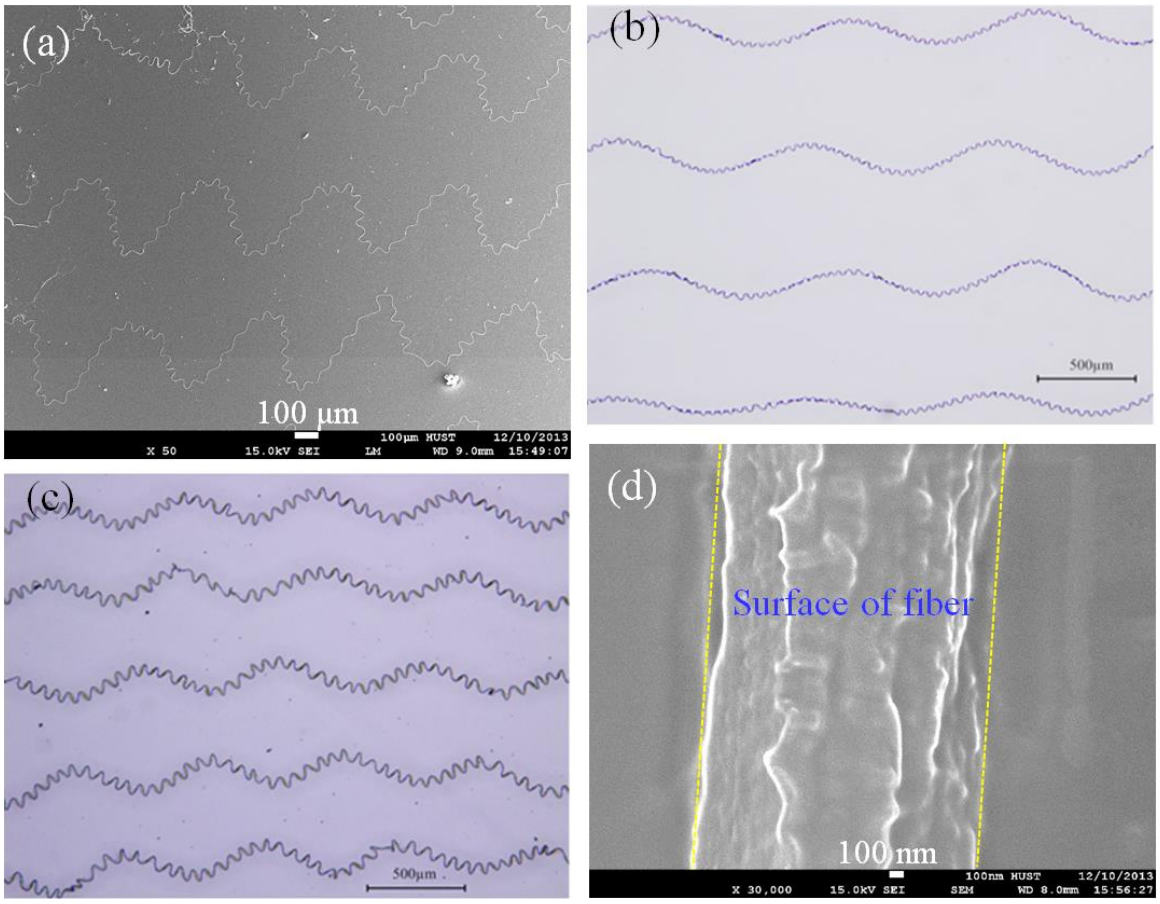

Supplementary Figure S6. SEM and optics figures of self-similar serpentine structures: (a) –(c) are self-similar serpentine structures with different wavelength and amplitude; (d) the surface morphology of the fiber. When $\bar{E}_{substrate} / E_{fiber} = 3.3\times10^{-4}$, the critical H/W is about 0.9. When H/W > 0.9, the fiber will buckle in the surface of the surface of elastomer substrate. The cross-section is about circle (H/W=1), which indicates that the fibers buckle in surface.

6. Direct-writing bead-on-string structures

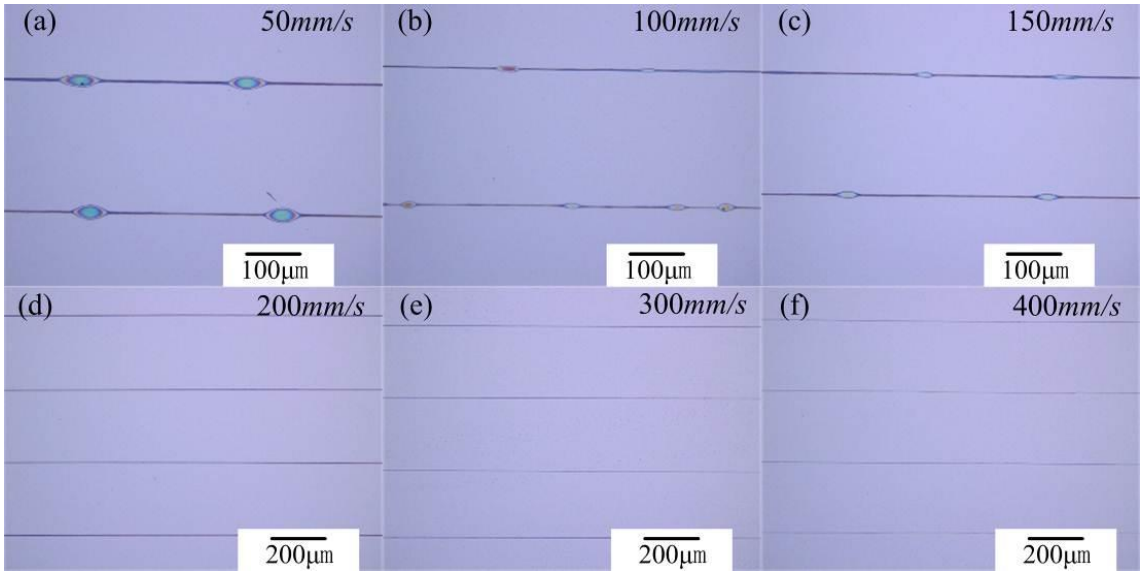

Supplementary Figure S7. Bead-on-string structures direct-written by Si-based multi-nozzle: (a) speed at 5 mm/s; (b) speed at 30 mm/s; (c) speed at 60 mm/s; (d) speed at 90 mm/s; (e) speed at 120 mm/s; (f) speed at 150 mm/s. The images of the lines generated at 2.2 kV.